nature climate change

LETTERS

PUBLISHED ONLINE: 8 JULY 2012 | DOI: 10.1038/NCLIMATE1589

Orbital forcing of tree-ring data

Jan Esper[1]*, David C. Frank[2,3], Mauri Timonen[4], Eduardo Zorita[5], Rob J. S. Wilson[6], Jürg Luterbacher[7], Steffen Holzkämper[1], Nils Fischer[8], Sebastian Wagner[5], Daniel Nievergelt[2,3], Anne Verstege[2,3] and Ulf Büntgen[2,3]

Solar insolation changes, resulting from long-term oscillations of orbital configurations[1], are an important driver of Holocene climate[2,3]. The forcing is substantial over the past 2,000 years, up to four times as large as the 1.6 W m^{-2} net anthropogenic forcing since 1750 (ref. 4), but the trend varies considerably over time, space and with season[5]. Using numerous high-latitude proxy records, slow orbital changes have recently been shown[6] to gradually force boreal summer temperature cooling over the common era. Here, we present new evidence based on maximum latewood density data from northern Scandinavia, indicating that this cooling trend was stronger (−0.31 °C per 1,000 years, ±0.03 °C) than previously reported, and demonstrate that this signature is missing in published tree-ring proxy records. The long-term trend now revealed in maximum latewood density data is in line with coupled general circulation models[7,8] indicating albedo-driven feedback mechanisms and substantial summer cooling over the past two millennia in northern boreal and Arctic latitudes. These findings, together with the missing orbital signature in published dendrochronological records, suggest that large-scale near-surface air-temperature reconstructions[9–13] relying on tree-ring data may underestimate pre-instrumental temperatures including warmth during Medieval and Roman times.

Over recent millennia, orbital forcing has continually reduced summer insolation in the Northern Hemisphere[5]. Peak insolation changes in Northern Hemisphere high latitudes, at ~65° N between June–August (JJA), have been identified as the prime forcing of climate variability over the past million years[1]. Together with long-term CO_2 variability resulting from biogeochemical feedbacks of the marine and terrestrial ecosystems[14], these insolation cycles have initiated the interplay between glacial and interglacial periods[15].

State-of-the-art coupled general circulation model (CGCM) simulations and high-resolution climate reconstructions rarely extend beyond the past few hundred years, limiting possibilities to evaluate low-frequency temperature fluctuations beyond broad assessments (and debate) of the Medieval Warm Period and Little Ice Age[4]. In fact, most high-resolution temperature reconstructions[16] including tree-ring width (TRW) records, the most widespread and important late-Holocene climate proxy[17], have never even been compared with orbital forcing. However, limitations related to the necessary removal of biological noise and the questioned ability of TRW records to reliably track recent (and past) warm episodes[18] may not make this proxy suitable to investigate the role of orbital forcing on climate. Indeed an evaluation of long-term temperature reconstructions, even over the past 7,000 years from across northern Eurasia, demonstrates that TRW-based records fail to show orbital signatures found in low-resolution proxy archives and climate model simulations (Supplementary Fig. S1). These discrepancies not only reveal that dendrochronological records are limited in preserving millennial scale variance, but also suggest that hemispheric reconstructions, integrating these data, might underestimate natural climate variability.

We here address these issues by developing a 2,000-year summer temperature reconstruction based on 587 high-precision maximum latewood density (MXD) series from northern Scandinavia (Fig. 1). The record was developed over three years using living and subfossil pine (*Pinus sylvestris*) trees from 14 lakes and 3 lakeshore sites >65° N (Methods), making it not only longer but also much better replicated than any existing MXD time series (for example, the widely cited Tornetraesk record contains 65 series[19]). We carried out a number of tests to the MXD network and noted the robustness of the long-term trends, but also the importance of including living trees from the lakeshore to form a seamless transition to the subfossil material preserved in the lakes (Methods). Calibration/verification with instrumental data is temporally robust and no evidence for divergence[20] was noted. The final reconstruction (N-scan) was calibrated against regional JJA temperature ($r_{1876–2006} = 0.77$) and spans the 138 BC–AD 2006 period.

N-scan shows a succession of warm and cold episodes including peak warmth during Roman and Medieval times alternating with severe cool conditions centred in the fourth and fourteenth centuries (Fig. 2). AD 21–50 (+1.05 °C, with respect to the 1951–1980 mean) was the warmest reconstructed 30-year period, ~2 °C warmer than the coldest AD 1451–1480 period (−1.19 °C) and still ~0.5 °C warmer than maximum twentieth-century warmth recorded AD 1921–1950 (+0.52 °C). Twentieth-century Scandinavian warming is relatively small compared with most other Northern Hemisphere high-latitude regions[4].

Superimposed on this interannual to multicentennial variability, N-scan reveals a long-term cooling trend of −0.31 °C per 1,000 years (±0.03 °C) over the 138 BC–AD 1900 period (the dashed red curve in Fig. 2) in line with evidence from low-resolution Holocene proxies[2,3]. The cooling trend, representing a −0.34 °C temperature difference between the first and second

[1]Department of Geography, Johannes Gutenberg University, 55099 Mainz, Germany, [2]Swiss Federal Research Institute WSL, 8903 Birmensdorf, Switzerland, [3]Oeschger Centre for Climate Change Research, University of Bern, 3012 Bern, Switzerland, [4]Finnish Forest Research Institute, Rovaniemi Research Unit, 96301 Rovaniemi, Finland, [5]Institute for Coastal Research, HZG Research Centre, 21494 Geesthacht, Germany, [6]School of Geography and Geosciences, University of St Andrews, St Andrews KY16 9AL, Scotland, UK, [7]Department of Geography, Climatology, Climate Dynamics and Climate Change, Justus-Liebig University, 35390 Giessen, Germany, [8]Max Planck Institute for Meteorology, 20146 Hamburg, Germany.
*e-mail: esper@uni-mainz.de.

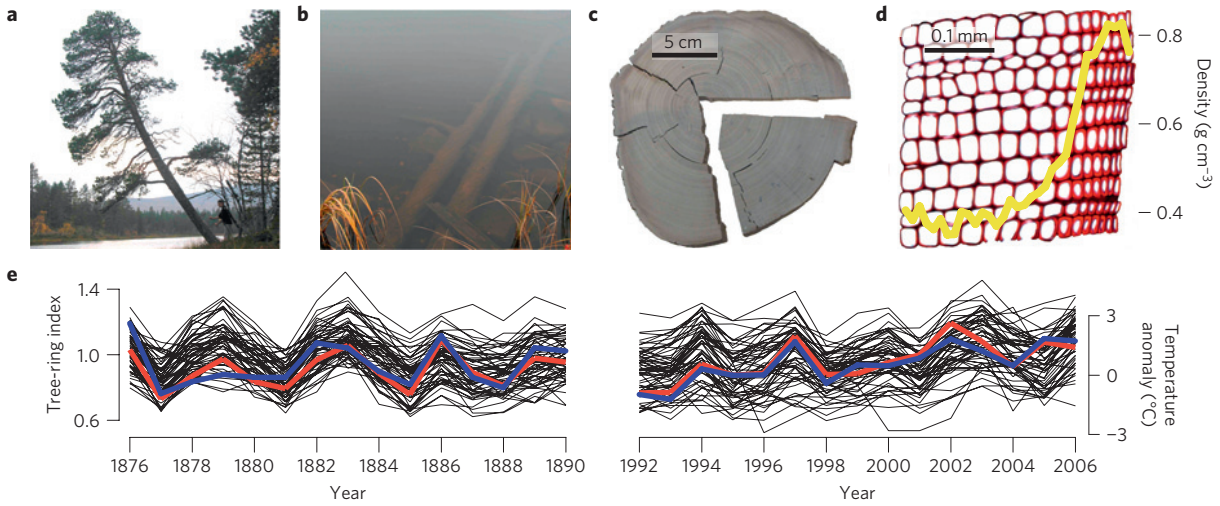

Figure 1 | High-precision density data derived from northern Scandinavian *P. sylvestris* trees. a,**b**, Core samples from living trees growing at lakeshores (**a**) were combined with submerged logs (**b**) to ensure MXD data homogeneity throughout the past two millennia. **c**, Stem disc obtained of a pine that fell nearly 1,500 years ago into Lake Riekkojärvi in northern Finland. The missing wedges show the two radii from which samples were taken for density measurements. The disc contains 176 annual rings dating AD 360–535. **d**, Photomicrograph of the AD 475 tree ring from **c**, together with a high-resolution density profile (yellow curve, in g cm^{-3}) derived from X-ray densitometry[28]. The density profile quantifies wood morphological changes throughout a growing season, from large and thin-walled earlywood cells (left) towards small and thick-walled latewood cells (right). Earlywood is laid down in the first weeks of the summer season, latewood develops over much of the high summer season. MXD in a given ring is reached towards the last cell row. The resolution of X-ray density profiles is 10 μm, the total width of the ring is 0.34 mm. **e**, Variability of MXD (grey curves) and instrumental temperature measurements (red and blue curves) over the earliest (AD 1876–1890) and latest (AD 1992–2006) 15-year periods common to these data. Tree-ring data were RCS-detrended, instrumental data are JJA mean temperatures with respect to a 1951–1980 reference period (Methods).

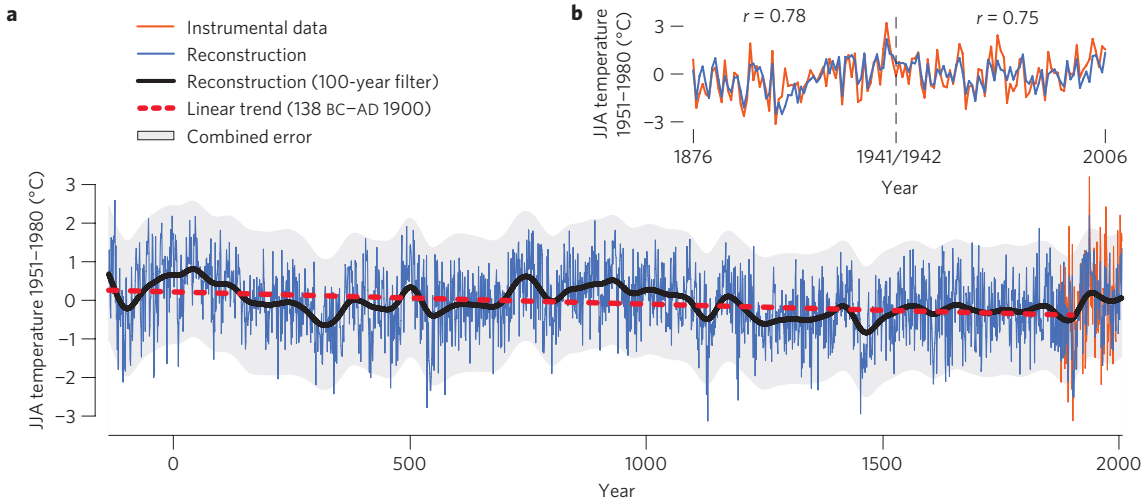

Figure 2 | N-scan JJA temperature reconstruction and fit with regional instrumental data. a, The reconstruction extends back to 138 BC highlighting extreme cool and warm summers (blue curve), cool and warm periods on decadal to centennial scales (black curve, 100-year spline filter) and a long-term cooling trend (dashed red curve; linear regression fit to the reconstruction over the 138 BC–AD 1900 period). Estimation of uncertainty of the reconstruction (grey area) integrates the validation standard error (±2 × root mean square error) and bootstrap confidence estimates. **b**, Regression of the MXD chronology (blue curve) against JJA temperatures (red curve) over the 1876–2006 common period. Correlations between MXD and instrumental data are 0.77 (full period), 0.78 (1876–1941 period), and 0.75 (1942–2006 period).

millennium AD (−0.36 °C excluding the twentieth century from the second millennium mean), is however not preserved in the TRW data from the same temperature-sensitive trees (Fig. 3). Similarly, no evidence for a long-term cooling trend is observed in a previous Fennoscandian TRW-based temperature reconstruction spanning the past 2,000 years[21]. Such a trend was found in only low-resolution lake sediment and ice-core data of a circum-Arctic proxy network[6]. The high-latitude TRW data included in ref. 6 also suggested no sign of a long-term cooling trend, demonstrating that variance at this lowest frequency is absent in existing tree-ring time series and thus most of the large-scale reconstructions produced so far[16]. Removal of the tree-ring data from the Arctic-wide network[6] results in an increased cooling trend substantially larger than the −0.21 °C per 1,000 years estimated using all proxy archives (Fig. 3c). Other reconstructions (besides the records shown here) that would be long enough and contain a clear and calibrated temperature signal to assess orbital signatures in tree-ring data are not available from the Northern Hemisphere at present.

As suggested previously[2,6], we propose that the millennial scale cooling trend retained in N-scan is forced by JJA insolation changes

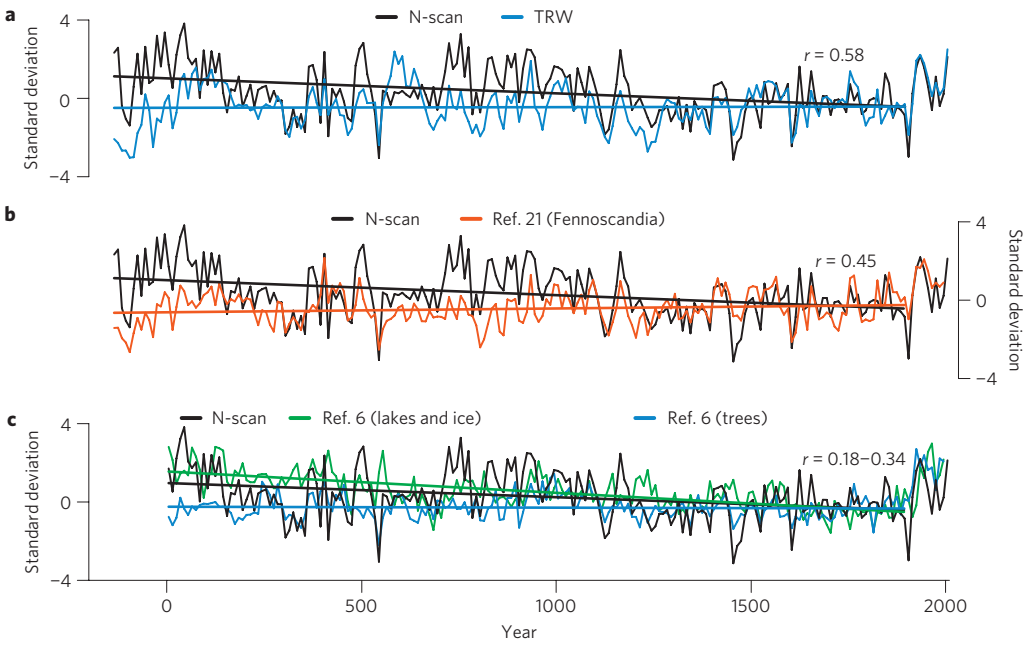

Figure 3 | Comparison of N-scan with decadally resolved Arctic proxy records. a, The MXD-based N-scan reconstruction plotted together with a RCS-detrended TRW chronology derived from the same wood samples. Records correlate at $r = 0.58$ over the 138 BC–AD 2006 common period. **b**, N-scan shown together with the long-term climate record from ref. 21 integrating existing tree-ring data from Finland and Sweden. Records correlate at $r = 0.45$ over the 138 BC–AD 1997 common period. **c**, N-scan together with mean time series from ref. 6 including a number of high-resolution Arctic proxy records from lakes and ice cores (green) and TRW (blue). Correlations between these records range from 0.18 to 0.34 over the AD 1–2000 common period. All time series are shown as ten-year means standardized relative to a 1500–2000 reference period.

of $\sim -6\,W\,m^{-2}$ over the past 2,000 years[5], as other potential forcings, including volcanic eruptions, land use and greenhouse gas changes, are either too small or free of long-term trends[4]. We tested this theory by analysing the two CGCMs that were run over several millennia (ECHO-G and ECHAM5–MPIOM; refs 7,8), and compared the modelled temperature trends with and without orbital forcing (Methods). The CGCMs revealed similar JJA temperature patterns including a long-term cooling trend over the past two millennia centred in Northern Hemisphere high latitudes (Supplementary Fig. S12). The cooling trends are stronger in the ECHO-G model (−0.19 °C per 1,000 years for the 60°–70° N latitudinal band) compared with the ECHAM5–MPIOM model (−0.10 °C per 1,000 years), but diminish in both CGCMs towards lower latitudes. A smaller trend in orbital forcing and reduced albedo-driven feedbacks from high-latitude terrestrial snow and sea-ice cover contribute to this latitudinal gradient (Supplementary Fig. S13; ref. 22). Both models reveal stronger cooling over the continents in comparison with the oceans and indicate trends of −0.17 °C (ECHO-G) and −0.10 °C (ECHAM5–MPIOM) per 1,000 years in the grid boxes closest to northern Scandinavia. Whereas the absolute values from the simulations might not be as reliable as the empirically derived estimates reported here (>−0.3° per 1,000 years in northern Scandinavia and the Arctic zone), the long-term CGCM runs are valuable for the spatial assessment of orbital signatures.

The missing millennial scale trends in existing TRW records as well as the increased cooling trend after removal of this proxy type from the Arctic-wide estimates[6] both suggest that the widely cited hemispheric reconstructions[9–14] underestimate pre-instrumental temperatures to some extent. This hypothesis seems to be important as most of the annually resolved, large-scale records are solely composed of or dominated (on longer timescales) by TRW data[16], and their spatial domain encompasses the Northern Hemisphere extratropics including northern boreal and Arctic environments. Inclusion of tree-ring data that lack millennial scale cooling trends, as revealed here (Fig. 3 and Supplementary Fig. S1), thus probably causes an underestimation of historic temperatures. In line with the course and magnitude of the underlying orbital forcing (Supplementary Fig. S13), this underestimation ought to build up back in time, for example from the Medieval back to Roman times. Impacts on large-scale reconstructions from the omitted long-term trend in tree-ring data should, however, diminish towards lower Northern Hemisphere latitudes, as the forcing and radiative feedbacks[5,22] decrease towards equatorial regions.

Further calculation of these effects based on the missing cooling trends in TRW data and the spatial CGCM temperature patterns is, however, not yet possible, as the existing large-scale reconstructions include changing regional proxies, represent varying fractions of Northern Hemisphere (full Northern Hemisphere, Northern Hemisphere extratropics, Northern Hemisphere high latitudes), and are composed and calibrated using an array of methods[16]. The implications of missing orbital signatures in tree-ring records are generally related to the overall variance of temperature variations retained in the large-scale reconstructions (Supplementary Fig. S14). Whereas most of these time series show a similar course of long-term temperature change—including warmth during Medieval times, cold during the Little Ice Age and subsequent warming—the magnitude of reconstructed temperatures differs considerably among the hemispheric records[16,23]. Some records show decadal scale variations of the order of ∼0.4 °C over the past millennium[12], whereas others indicate temperature variability up to 1.0 °C over the same period[9]. As a consequence, any adjustment for the omitted millennial scale temperature trends in dendrochronological records would have stronger implications, if the calibrated amplitude of past temperature variations was indeed small, say <0.5 °C, but would be less significant if the high-variance reconstructions turn out to be correct. The missing orbital signature in tree-ring records is also less significant to reconstructions containing variance increases (owing to reduced proxy coverage) back in time[9,13]. These results reinforce the need to better constrain the pre-instrumental temperature variance structure[10] and amplitude[23].

Whereas our results on orbitally forced climate trends in a 2,000-year MXD chronology seem to be in line with coarse-resolution Holocene proxies[2,3] and are supported by CGCM evidence[7,8], little attention has been paid to the lack of these trends in long-term tree-ring records and implications thereof. The JJA temperature reconstruction presented here closes this gap, a finding that largely stems from the exceptionally strong and temporally stable climate signal, and the unprecedented length and replication of the new N-scan MXD chronology. The ability of MXD data to retain millennial scale temperature trends seems to result from a number of properties, including a reduced age trend[24] and biological persistence[25] resulting in less distortion of retained trends through regional curve standardization[26] (RCS), the ability of tree populations to develop cell walls of continuously changing thickness over millennia and the non-plastic response of the termination of cell-wall lignification with respect to the integrated heat over the high and late summer seasons[27]. It is the combination of these properties that seems to enable the retention of a millennial scale trend in the MXD record and the lack of this lowest frequency variance in existing TRW records. These findings together with the trends revealed in long-term CGCM runs suggest that large-scale summer temperatures were some tenths of a degree Celsius warmer during Roman times than previously thought.

It has been demonstrated[4] that prominent, but shorter term climatic episodes, including the Medieval Warm Period and subsequent Little Ice Age, were influenced by solar output and (grouped) volcanic activity changes, and that the extent of warmth during medieval times varies considerably in space. Regression-based calculations over only the past millennium (including the twentieth century) are thus problematic as they effectively provide estimates of these forcings that typically act on shorter timescales. Accurate estimation of orbitally forced temperature signals in high-resolution proxy records therefore requires time series that extend beyond the Medieval Warm Period and preferably reach the past 2,000 years or longer[6].

Further uncertainty on estimating the effect of missing orbital signatures on hemispheric reconstructions is related to the spatial patterns of JJA orbital forcing and associated CGCM temperature trends. First, the simulated temperature trends, indicating substantial weakening of insolation signals towards the tropics, can at present be assessed in only two CGCMs (refs 7,8). More long-term runs with GCMs to validate these hemispheric patterns are required. Whereas the large-scale patterns of temperature trends seem rather similar among the CGCMs, the magnitude of orbitally forced trends varies considerably among the simulations. Additional uncertainty stems from the weight of tree-ring data and varying seasonality of reconstructed temperatures in the large-scale compilations. Although some of the reconstructions are solely composed of tree-ring data, others include a multitude of proxies (including precipitation-sensitive time series) and may even include non-summer temperature signals. Some of these issues are difficult to tackle, as the weighting of individual proxies in several large-scale reconstructions is poorly quantified. The results presented here, however, indicate that a thorough assessment of the impact of potentially omitted orbital signatures is required as most large-scale temperature reconstructions include long-term tree-ring data from high-latitude environments. Further well-replicated MXD-based reconstructions are needed to better constrain the orbital forcing of millennial scale temperature trends and estimate the consequences to the ongoing evaluation of recent warming in a long-term context.

Methods

Tree-ring data and spatial coherence. We collected core samples from living *P. sylvestris* trees growing at lakeshore and inland (that is ten or more metres distance from lakes) microsites, and disc samples from submerged logs in northern Finland and Sweden (Supplementary Table S1 and Fig. S2). MXD data were derived from high-resolution density profiles using X-ray radiographic techniques[28] (Fig. 1). Within and between-site coherence of the northern Scandinavian MXD network has been assessed using a total of nine data sets from living trees—of which three (Ket, Kir, Tor) are additionally subdivided into lakeshore and inland subsets—and 14 data sets from subfossil lake material. We calculated Pearson correlation coefficients among living-tree chronologies over the 1812–1978 common period ($r_{MXD} = 0.72$, $r_{TRW} = 0.58$; Supplementary Table S2 and Fig. S3), and over varying periods of overlap (AD 700–1600) between subfossil MXD chronologies ($r_{MXD} = 0.71$; Supplementary Table S3 and Fig. S4) to estimate data homogeneity throughout space and time. To ensure signal homogeneity, we considered MXD data from only lakeshore sites together with the subfossil material discovered from the lakes for the final reconstruction (N-scan). The record integrates 587 high-resolution *P. sylvestris* MXD measurement series.

Chronology development and assessment. Various combinations of living-tree and subfossil MXD data were produced to assess the sensitivity of the long-term N-scan record to detrending methodology and microsite conditions. Application of negative exponential and RCS detrending techniques revealed substantial changes in retained low-frequency variance and sensitivity of twentieth-century trends to density differences between living-tree sites ranging from ~0.002 to 0.010 g cm^{-3} over the first 200 years of tree growth (Supplementary Fig. S5). Sensitivity of increased (decreased) twentieth-century chronology levels was assessed using MXD data from only lakeshore (inland) microsites in long-term RCS runs (Supplementary Fig. S6). N-scan characteristics were detailed by calculating 95% bootstrap confidence ranges, chronology age and replication curves, and interseries correlation and expressed population signal statistics (Supplementary Fig. S7). We analysed the RCS detrended N-scan data by classifying the measurement series into age classes ranging from 1–10 years to 201–210 years and calculating 100-year spline filters for each of these classes (Supplementary Fig. S8). This procedure provided insights into the coherence of long-term trends retained in (typically noisier) juvenile and (typically less replicated) adult tree-ring data. N-scan trend behaviour was additionally assessed by analysing the persistence of low-frequency variability in tree-ring parameters, indicating that only the MXD data preserved substantial variance on millennial timescales (Supplementary Fig. S9).

Proxy calibration and JJA temperature reconstruction. The MXD climate signal was assessed using Pearson correlation coefficients between the lakeshore subsets Ket-L ($r = 0.74$), Kir-L ($r = 0.75$) and Tor-L ($r = 0.74$) and mean JJA temperatures recorded at the global historical climatology network stations Haparanda, Karasjok and Sodankyla over the 1876–2006 common period. Running correlations were applied to analyse the temporal characteristics of the signal revealing reduced coherence among the station records as well as between the station and proxy data centred in the 1910s (Supplementary Fig. S10). The long-term N-scan record integrating lakeshore and subfossil MXD data correlates at 0.77 ($r^2 = 0.59$) with regional JJA temperatures. We transferred this record into a JJA temperature reconstruction using ordinary least square regression with MXD as the independent variable. This approach provides conservative estimates—owing to the reduction of variability caused by unexplained variance[29]—of pre-instrumental climate variability and derived long-term trends. Split-period calibration/verification statistics[30] with early and late r^2 (0.-57–0.61), reduction of error (0.57–0.59), coefficient of efficiency (0.50–0.54) and full period Durbin–Watson (1.75) statistics were applied to validate the reconstruction. N-scan confidence intervals were calculated considering the standard error (±2 × root mean square error) derived from verification against instrumental JJA temperatures over the early 1876–1941 period and a bootstrap confidence range derived from resampling the MXD data 1,000 times with replacement. A total of 2,000 MXD chronologies derived from randomly drawn subsets of the N-scan record were developed to test the influence of reduced sample replication, typical to earlier periods of the long-term reconstruction, on the calibration results. These tests revealed that the transfer model remains robust ($r > 0.70$) down to a replication of ten MXD measurement series (Supplementary Fig. S11). Extreme cool and warm summers (decades and centuries) since 138 BC are expressed as deviations from the 1951 to 1980 mean (Supplementary Table S4) and millennial scale JJA temperature trends estimated by calculating a linear ordinary least square regression over the 138 BC–AD 1900 period (Fig. 2). The robustness of the regression slope (−0.31 °C per 1,000 years) was tested by reducing the length of the regression period stepwise at both ends by 100 years to derive a 95% confidence range (±0.03 °C) of the millennial scale trend.

CGCM Holocene simulations. Spatial patterns of JJA surface air temperatures derived from multimillennial ECHO-G (ref. 7) and ECHAM5–MPIOM (ref. 8) CGCM runs forced with and without long-term insolation changes were analysed to estimate low-frequency temperature trends throughout the Northern Hemisphere extratropics (Supplementary Fig. S12). ECHO-G is one of the coupled atmosphere–ocean models considered in the Intergovernmental Panel on Climate Change Fourth Assessment Report and was ranked among the best five models in simulating the mean patterns of surface atmospheric circulation and precipitation[4]. It integrates the atmospheric ECHAM4 model with a horizontal resolution of 3.75 × 3.75 degrees and 19 vertical levels, and the oceanic HOPE model with a

horizontal resolution ranging from about 2.8 × 2.8 to 0.5 × 0.5 degrees towards the Equator and 20 vertical levels including a thermodynamic sea-ice model. To avoid artificial climate drift in the very long (7,000 years) climate simulations used here, a flux adjustment was applied to the atmosphere–ocean coupling. The second transient Holocene simulation[8] consists of the spectral atmosphere model ECHAM5 run at truncation T31, corresponding to a horizontal resolution of a 3.75 × 3.75 longitude–latitude grid, with 19 vertical hybrid sigma pressure levels and the highest level at 10 hPa. It integrates the land-surface model JSBACH including a dynamic vegetation module, has been coupled to the ocean GCM MPIOM run with 40 vertical levels (30 levels within the top 2,000 m) and includes a zero-layer dynamic-thermodynamic sea-ice model with viscous-plastic rheology. No flux correction has been applied to this CGCM.

Received 27 March 2012; accepted 15 May 2012; published online 8 July 2012

References

1. Milankovitch, M. *Kanon der Erdbestrahlung und seine Anwendung auf das Eiszeitenproblem.* (Königlich Serbische Akademie, 1941).
2. Wanner, H. *et al.* Mid- to late Holocene climate change: An overview. *Quat. Sci. Rev.* **27,** 1791–1828 (2008).
3. Mayewski, P. A. *et al.* Holocene climate variability. *Quat. Res.* **62,** 243–255 (2004).
4. IPCC *Climate Change 2007: The Physical Science Basis* (eds Solomon, S. *et al.*) (Cambridge Univ. Press, 2007).
5. Berger, A. & Loutre, M. F. Insolation values for the climate of the last 10 million years. *Quat. Sci. Rev.* **10,** 297–317 (1991).
6. Kaufman, D. S. *et al.* Recent warming reverses long-term Arctic cooling. *Science* **325,** 1236–1339 (2009).
7. Zorita, E., Gonzlez-Rouco, F., von Storch, H., Montavez, J. P. & Valero, F. Natural and anthropogenic modes of surface temperature variations in the last thousand years. *Geophys. Res. Lett.* **32,** L08707 (2005).
8. Fischer, N. & Jungclaus, J. H. Evolution of the seasonal temperature cycle in a transient Holocene simulation: Orbital forcing and sea-ice. *Clim. Past* **7,** 1139–1148 (2011).
9. Esper, J., Cook, E. & Schweingruber, F. Low-frequency signals in long tree-ring chronologies for reconstructing past temperature variability. *Science* **295,** 2250–2253 (2002).
10. Frank, D., Esper, J. & Cook, E. R. Adjustment for proxy number and coherence in a large-scale temperature reconstruction. *Geophys. Res. Lett.* **34,** L16709 (2007).
11. Hegerl, G. C. *et al.* Detection of human influence on a new, validated 1500-year temperature reconstruction. *J. Clim.* **20,** 650–666 (2007).
12. Mann, M. E., Bradley, R. S. & Hughes, M. K. Northern hemisphere temperatures during the past millennium: Inferences, uncertainties, and limitations. *Geophys. Res. Lett.* **26,** 759–762 (1999).
13. Mann, M. E. *et al.* Proxy-based reconstructions of hemispheric and global surface temperature variations over the past two millennia. *Proc. Natl Acad. Sci. USA* **105,** 13252–13257 (2008).
14. Frank, D. C. *et al.* Ensemble reconstruction constraints on the global carbon cycle sensitivity to climate. *Nature* **463,** 527–530 (2010).
15. Laepple, T., Werner, M. & Lohmann, G. Synchronicity of Antarctic temperatures and local solar insolation on orbital timescales. *Nature* **471,** 91–94 (2011).
16. Frank, D., Esper, J., Zorita, E. & Wilson, R. A noodle, hockey stick, and spaghetti plate: A perspective on high-resolution paleoclimatology. *Wiley Interdiscipl. Rev. Clim. Change* **1,** http://dx.doi.org/10.1002/wcc.53(2010).
17. Esper, J., Frank, D. C. & Wilson, R. J. S. Climate reconstructions: Low frequency ambition and high frequency ratification. *Eos* **85,** 113, 130 (2004).
18. Cook, E. R., Briffa, K. R., Meko, D. M., Graybill, D. A. & Funkhouser, G. The 'segment length curse' in long tree-ring chronology development for palaeoclimatic studies. *Holocene* **5,** 229–237 (1995).
19. Schweingruber, F. H., Bartholin, T., Schär, E. & Briffa, K. R. Radiodensitometric-dendroclimatological conifer chronologies from Lapland (Scandinavia) and the Alps (Switzerland). *Boreas* **17,** 559–566 (1988).
20. Esper, J. *et al.* Trends and uncertainties in Siberian indicators of 20th century warming. *Glob. Change Biol.* **16,** 386–398 (2010).
21. Briffa, K. R. *et al.* Trends in recent temperature and radial tree growth spanning 2000 years across northwest Eurasia. *Philos. Trans. R. Soc. B* **363,** 2269–2282 (2008).
22. Kerwin, M. W. *et al.* The role of oceanic forcing in mid-Holocene northern hemisphere climatic change. *Paleoceanography* **14,** 200–210 (1999).
23. Esper, J. *et al.* Climate: Past ranges and future changes. *Quat. Sci. Rev.* **24,** 2164–2166 (2005).
24. Frank, D. & Esper, J. Characterization and climate response patterns of a high-elevation, multi-species tree-ring network for the European Alps. *Dendrochronologia* **22,** 107–121 (2005).
25. Frank, D., Büntgen, U., Böhm, R., Maugeri, M. & Esper, J. Warmer early instrumental measurements versus colder reconstructed temperatures: Shooting at a moving target. *Quat. Sci. Rev.* **26,** 3298–3310 (2007).
26. Esper, J., Cook, P. J., Krusic, K., Peters, F. H. & Schweingruber, Tests of the RCS method for preserving low-frequency variability in long tree-ring chronologies. *Tree-Ring Res.* **59,** 81–98 (2003).
27. Moser, L. *et al.* Timing and duration of European larch growing season along an altitudinal gradient in the Swiss Alps. *Tree Physiol.* **30,** 285–233 (2010).
28. Schweingruber, F. H., Fritts, H. C., Bräker, O. U., Drew, L. G. & Schaer, E. The X-ray technique as applied to dendroclimatology. *Tree-Ring Bull.* **38,** 61 (1978).
29. Lee, T., Zwiers, F. & Tsao, M. Evaluation of proxy-based millennial reconstruction methods. *Clim. Dynam.* **31,** 263–281 (2008).
30. Cook, E. R., Briffa, K. & Jones, P. D. Spatial regression methods in dendroclimatology: A review and comparison of techniques. *Int. J. Climatol.* **14,** 379–402 (1994).

Acknowledgements

We thank D. S. Kaufman for comments and H. Grudd for help with fieldwork. Supported by the Mainz Geocycles Research Centre and Palaeoweather Group, the European Union projects Carbo-Extreme (226701), CIRCE (36961) and ACQWA (212250), the Swiss National Science Foundation project INTEGRAL (121859), the German Science Foundation project PRIME (LU1608/1-1) and the Eva Mayr-Stihl Foundation.

Author contributions

J.E., D.C.F., M.T., E.Z., R.J.S.W. and U.B. designed the study. Field sampling and measurements were done by J.E., D.C.F., M.T., R.J.S., U.B., D.N. and A.V. J.E., D.C.F., E.Z. and U.B. carried out the analysis with input from R.J.S., J.L., S.H., N.F. and S.W. All authors contributed to discussion, interpretation and writing the paper.

Additional information

The authors declare no competing financial interests. Supplementary information accompanies this paper on www.nature.com/natureclimatechange. Reprints and permissions information is available online at www.nature.com/reprints. Correspondence and requests for materials should be addressed to J.E.

nature climate change

SUPPLEMENTARY INFORMATION

DOI: 10.1038/NCLIMATE1589

SUPPLEMENTARY INFORMATION
INCLUDING 4 SUPPLEMENTARY TABLES, AND 14 SUPPLEMENTARY FIGURES

Orbital forcing of tree-ring data

Jan Esper[1], David C. Frank[2], Mauri Timonen[3], Eduardo Zorita[4], Rob J. S. Wilson[5], Jürg Luterbacher[6], Steffen Holzkämper[1], Nils Fischer[7], Sebastian Wagner[4], Daniel Nievergelt[2], Anne Verstege[2], Ulf Büntgen[2]

[1]Department of Geography, Johannes Gutenberg University, 55099 Mainz, Germany. [2]Swiss Federal Research Institute WSL, 8903 Birmensdorf & Oeschger Centre for Climate Change Research, University of Bern, 3012 Bern, Switzerland. [3]Finnish Forest Research Institute, Rovaniemi Research Unit, 96301 Rovaniemi, Finland. [4]Institute for Coastal Research, HZG Research Centre, 21494 Geesthacht, Germany. [5]School of Geography and Geosciences, University of St Andrews, St Andrews, KY16 9AL, Scotland, UK. [6]Department of Geography, Climatology, Climate Dynamics and Climate Change, Justus-Liebig University, 35390 Giessen, Germany. [7]Max Planck Institute for Meteorology, 20146 Hamburg, Germany
**e-mail: esper@uni-mainz.de*

Table S1. *Tree-ring sampling sites and basic MXD data summary statistics. For site locations see Fig. S2.*

Location	Lon.	Lat.	Elevation	No. Series	Start	End	MSL*	Rbar**
Living-tree sites								
Ala	30.00	66.00	200	33	1699	1992	268	0.45
Kes	24.30	67.56	450	99	1475	2006	269	0.41
Ket	24.05	68.22	300	198	1596	2006	160	0.41
Kir	20.10	67.90	430	191	1656	2006	96	0.47
Laa	27.07	67.00	320	21	1670	1978	235	0.51
Luo	24.15	67.50	300	128	1653	2006	139	0.34
Mur	32.00	68.00	140	32	1715	1992	250	0.57
Tor	19.80	68.20	390	176	1799	2006	76	0.45
Tor(old)	19.40	68.14	400	65	441	1980	290	0.38
Mean	*24.54*	*67.61*	*326*	*105*	*1523*	*1997*	*198*	*0.44*
Lakeshore micro-sites								
Ket-L	24.05	68.22	300	49	1596	2006	167	0.47
Kir-L	20.10	67.90	430	87	1656	2006	84	0.46
Tor-L	19.80	68.20	390	79	1800	2006	59	0.45
Mean	*21.32*	*68.11*	*373*	*72*	*1684*	*2006*	*103*	*0.46*
Inland micro-sites								
Ket-I	24.05	68.22	300	66	1572	2006	141	0.37
Kir-I	20.10	67.90	430	104	1775	2006	105	0.49
Tor-I	19.80	68.20	390	97	1796	2006	88	0.45
Mean	*21.32*	*68.11*	*373*	*89*	*1714*	*2006*	*111*	*0.44*
Sub-fossil sites								
Aka	24.20	67.70	265	8	1311	1782	137	0.49
Hae	27.50	67.50	290	2	1342	1533	126	0.85
Hal	29.00	66.80	290	6	691	1282	144	0.63
Kal	24.80	68.50	340	10	271	1553	180	0.42
Koi	27.50	68.70	250	10	48 BC	1767	149	0.65
Kol	29.00	66.80	293	6	1686	1916	175	0.62
Kom	28.00	68.50	190	83	216 BC	1906	182	0.36
Kul	23.00	68.50	334	49	488	1704	144	0.47
Luo	28.00	68.50	200	68	5 BC	1897	183	0.31
Nak	23.50	68.70	330	37	372	1822	107	0.37
Pel	24.80	68.50	337	5	171	1743	141	0.34
Pet	27.00	69.50	190	10	883	1792	118	0.50
Pit	27.50	67.50	290	16	7 BC	1749	103	0.67
Rie	28.00	68.50	190	59	301	1770	176	0.43
Mean	*26.56*	*68.16*	*271*	*26*	*517*	*1730*	*148*	*0.51*

* MSL is mean series length.
** Rbar is the mean inter-series correlation of the raw MXD timeseries.

Table S2. *Coherence among northern Scandinavian Pinus sylvestris MXD and TRW datasets. The table lists the correlations between TRW (bottom left) and MXD (top right) chronologies over the 1812-1978 common period. Bold values are the average correlations for each site. Average correlation between all MXD sites is 0.72, and 0.58 for all TRW sites. TRW and MXD data were detrended by calculating ratios from negative exponential functions, and mean chronologies developed using the arithmetic mean.*

	Ala	Kes	Ket	Kir	Laa	Luo	Mur	Tor	Tor(old)	**Mean**
Ala		0.65	0.71	0.60	0.75	0.47	0.74	0.57	0.61	**0.64**
Kes	0.63		0.90	0.83	0.83	0.85	0.59	0.77	0.77	**0.77**
Ket	0.50	0.68		0.88	0.83	0.80	0.66	0.82	0.77	**0.80**
Kir	0.62	0.67	0.83		0.70	0.76	0.57	0.92	0.84	**0.76**
Laa	0.62	0.69	0.48	0.51		0.72	0.68	0.65	0.68	**0.73**
Luo	0.01	0.45	0.52	0.41	0.38		0.47	0.70	0.64	**0.68**
Mur	0.69	0.52	0.54	0.64	0.57	0.31		0.56	0.59	**0.61**
Tor	0.63	0.65	0.75	0.84	0.52	0.34	0.66		0.85	**0.73**
Tor(old)	0.54	0.63	0.64	0.84	0.55	0.42	0.64	0.87		**0.72**
Mean	**0.53**	**0.61**	**0.62**	**0.67**	**0.54**	**0.35**	**0.57**	**0.65**	**0.64**	

Table S3. *Coherence within and between sub-fossil datasets from lakes in northern Scandinavia. The table lists within-site and inter-site correlations calculated for a total of 12 periods covered by RCS chronologies with minimum replications > 9 MXD measurement series (see Fig. S4). These requirements are met at lakes Kom, Kul, Luo, Nak, and Rie. All data were RCS-detrended on a site-by-site basis.*

Period	Length	Within-site correlation					Inter-site correlation
		Kom	Kul	Luo	Nak	Rie	
756-971	216	0.40		0.35			0.71
937-970	34			0.48		0.58	0.81
937-997	61	0.39				0.55	0.75
1175-1190	16	0.36				0.38	0.88
1285-1287	3	0.32				0.52	0.74
1297-1311	15	0.28	0.59				0.21
1314-1419	106		0.55	0.37			0.65
1499-1506	8		0.49		0.08		0.62
1519-1525	7		0.32		0.32		0.74
1530-1559	30	0.55			0.31		0.74
1547-1559	13				0.19		0.92
1547-1566	20	0.46					0.79

Table S4. *JJA temperature deviations from the 1951-1980 mean in the 10 coldest and warmest reconstructed years, decades, and centuries since 138 BC. All values derived from the N-Scan JJA temperature reconstruction.*

	Rank	Year	°C	Decade	°C	Century	°C
warmest	1.	125 BC	2.59	AD 41-50	1.34	1st AD	0.60
	2.	AD 1937	2.20	10-1 BC	1.56	8th AD	0.37
	3.	4 BC	2.18	AD 701-710	1.21	1st BC	0.37
	4.	AD 46	2.17	AD 31-40	1.10	9th AD	0.30
	5.	54 BC	2.11	30-21 BC	1.01	10th AD	0.30
	6.	AD 34	2.07	AD 501-510	0.94	11th AD	0.19
	7.	AD 891	2.06	AD 721-730	0.93	2nd AD	0.11
	8.	26 BC	2.00	60-51 BC	0.86	18th AD	-0.06
	9.	AD 493	1.92	AD 771-780	0.85	20th AD	-0.06
	10.	AD 1831	1.86	121-130 BC	0.84	5th AD	-0.07
coldest	1.	AD 1130	-3.12	AD 1451-1460	-1.47	16th AD	-1.06
	2.	AD 1453	-2.94	AD 541-550	-1.43	14th AD	-0.51
	3.	AD 536	-2.78	AD 1901-1910	-1.41	13th AD	-0.49
	4.	AD 1194	-2.58	AD 1601-1610	-1.19	15th AD	-0.45
	5.	AD 1904	-2.52	AD 1461-1479	-1.11	4th AD	-0.39
	6.	AD 1902	-2.47	AD 1471-1480	-1.01	17th AD	-0.27
	7.	AD 574	-2.44	AD 411-420	-0.98	19th AD	-0.26
	8.	AD 1127	-2.43	AD 11211230	-0.95	12th AD	-0.21
	9.	AD 339	-2.42	AD 301-310	-0.93	6th AD	0.14
	10.	AD 543	-2.34	AD 351360	-0.90	7th AD	-0.14

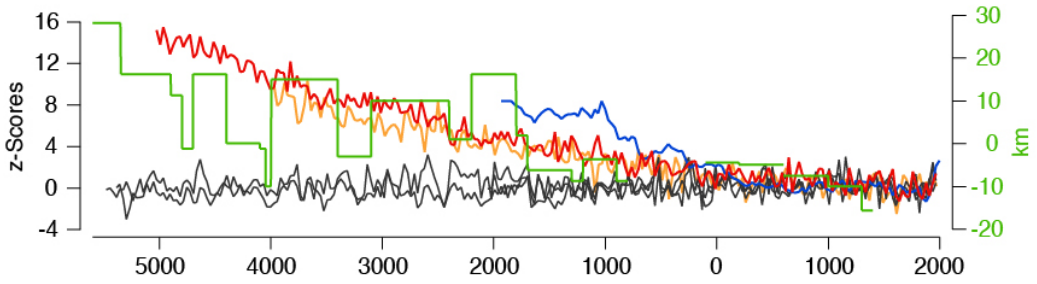

Figure S1. *Temperature trends recorded over the past 4000-7000 years in high latitude proxy and CGCM data. Multi-millennial TRW records from Sweden[1], Finland[2], and Russia[3] (all in grey) together with reconstructions of the glacier equilibrium line in Norway[4,5] (blue), northern treeline in Russia[3,6] (green), and JJA temperatures in the 60-70°N European/Siberian sector from orbitally forced ECHO-G[7,8] (red) and ECHAM5/MPIOM[9] (orange) CGCM runs[10]. All records, except for the treeline data (in km) were normalized relative to the AD 1500-2000 period. Resolution of model and TRW data were reduced (to ~ 30 years) to match the glacier data.*

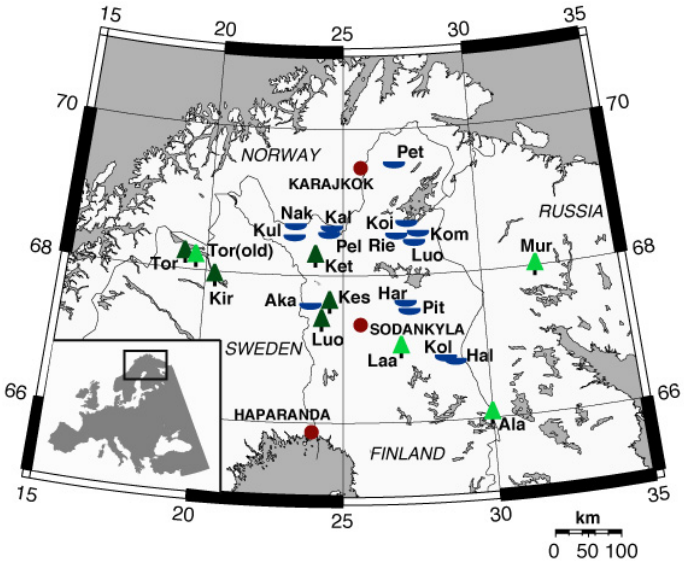

Figure S2. *Map showing the Pinus sylvestris tree-ring density network and long-term meteorological stations in Northern Scandinavia. Tree symbols indicate living-tree sites sampled in 2007 (dark green) and in the late 20th century (light green) by WSL staff. Blue symbols indicate lake sites from which sub-fossil trees were collected by Metla staff and high-precision density profiles measured over the past three years. Meteorological stations where observations started before 1910 are shown in red.*

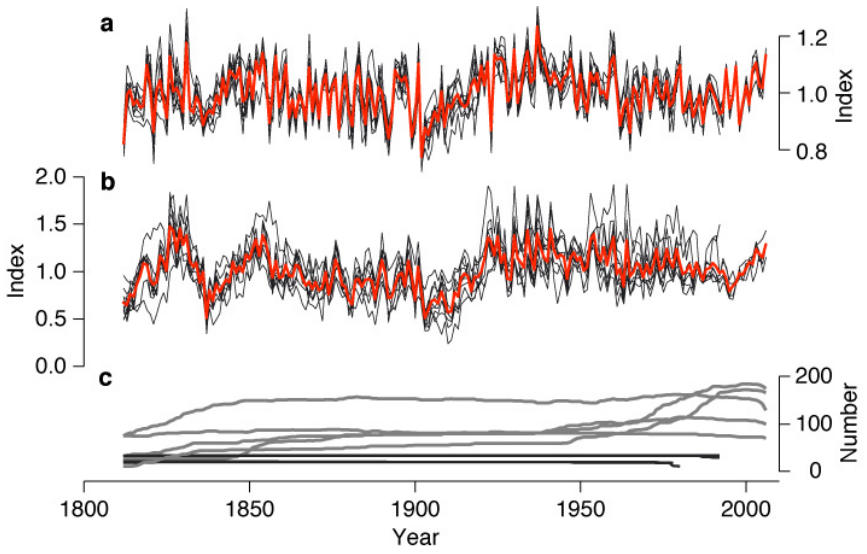

Figure S3. *Coherence between northern Scandinavian tree-ring records.* ***a****, MXD and* ***b****, TRW chronologies from sites Ala, Kes, Ket, Kir, Laa, Luo, Mur, Tor, and TorOld back to AD 1812. Red curve is the arithmetic mean of the site records. Tree-ring data were detrended using negative exponential growth curves.* ***c****, Number of measurement series integrated in each site record, with black curves indicating replication in Ala, Laa, Mur, and TorOld extending into the late 1980s and early 1990s, and grey curves indicating replication in Kes, Ket, Kir, Luo, and Tor extending until 2006 (see Table S1). Minimum replication of 10 samples is reached in Tor in 1812.*

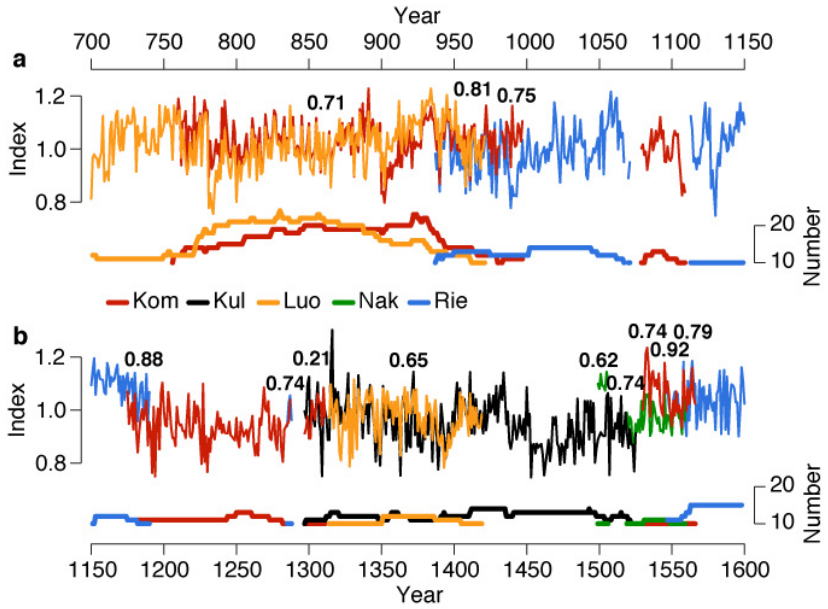

Figure S4. *Coherence of sub-fossil MXD data from different lakes in northern Scandinavia. Segments of MXD mean chronologies that include 10 or more radii (see replication curves at the bottom of the panels) are shown for* ***a****, the AD 700-1150 and* ***b****, the AD 1150-1600 periods. This sample replication is reached in five lakes (Kom, Kul, Luo, Nak, Rie). Bold numbers indicate the correlation between individual chronology segments over various periods of overlap (see Table S3 for details). All tree-ring data were detrended using RCS on a site-by-site basis.*

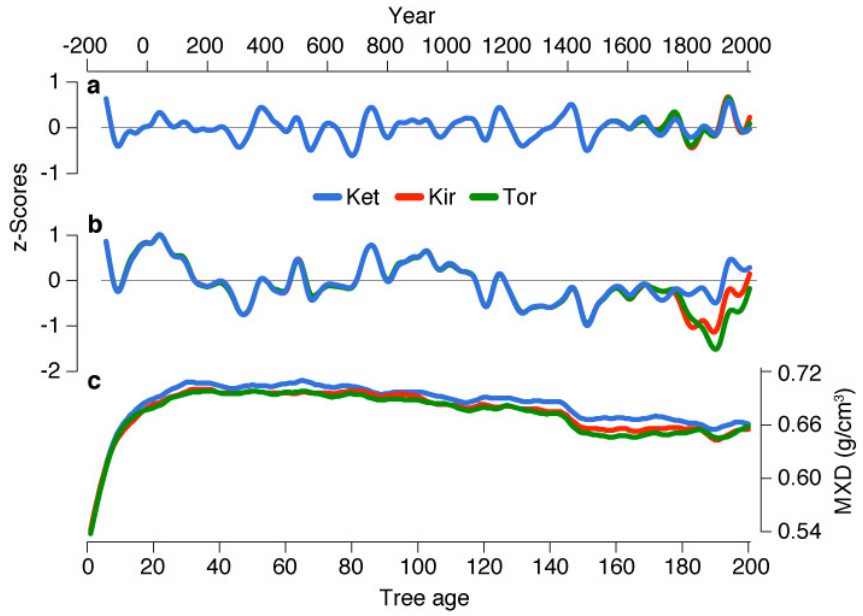

Figure S5. *Influence of detrending and sampling site on the shape of the long-term N-Scan record. Comparison of chronologies integrating living trees from sites Ket, Kir, and Tor, after* ***a****, negative exponential and* ***b****, RCS detrending[11]. Records were normalized over the 138 BC to AD 1600 period, and smoothed using a 100-year spline filter.* ***c****, Ten-year smoothed mean curves of the age-aligned MXD data (the `regional curves´) of the chronologies displayed in* ***a*** *and* ***b****. Regional curves are shown over the well-replicated (>100 samples) first 200 years.*

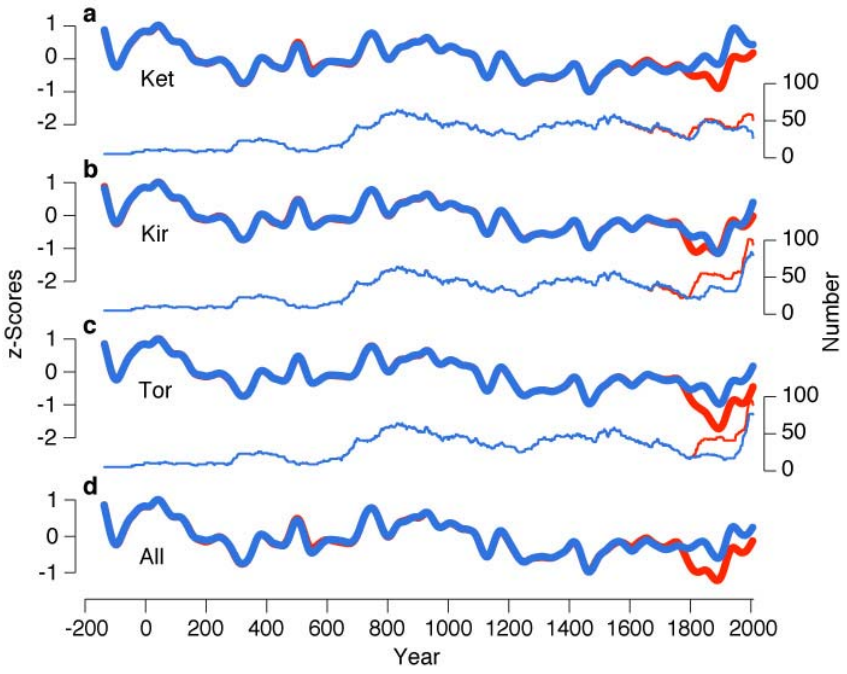

Figure S6. *Influence of micro-site conditions on the shape of the long-term N-Scan record. Comparison of chronologies integrating living trees sampled at lakeshores (blue) and inland (red). Results from* ***a****, Ket* ***b****, Kir* ***c****, Tor, and* ***d****, a run using all data from these sites are shown. Records were normalized over the 138 BC to AD 1600 period, and smoothed using a 100-year spline filter. Thin curves show sample replication changes of the historic and recent (lakeshore and inland) material.*

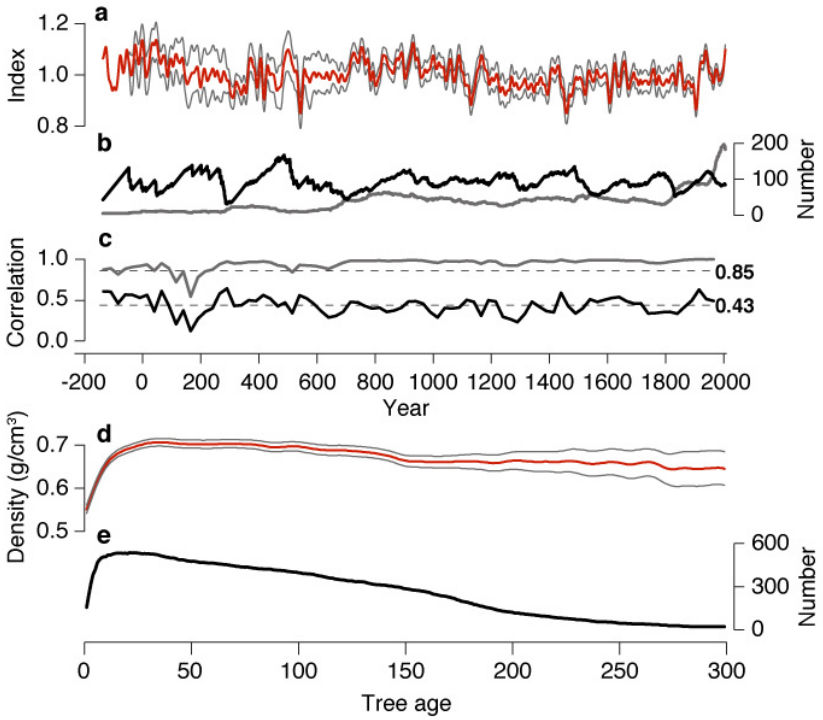

Figure S7. *N-Scan tree-ring chronology and summary statistics.* ***a****, The RCS-detrended MXD chronology (red) shown together with the 95% bootstrap confidence range (grey)[11]. Timeseries are smoothed using a 20-year spline filter.* ***b****, The mean chronology age (black) and number of MXD measurement series (grey) calculated for each year over the 138 BC to AD 2006 period.* ***c****, The expressed population signal (EPS in grey)[12] and the mean inter-series correlation (Rbar in black) calculated over 50-year periods shifted stepwise by 25-years along the chronology. The widely cited EPS value of 0.85 and mean Rbar (0.43) are indicated by dashed lines.* ***d****, The 20-year smoothed mean timeseries of all MXD measurement series after alignment by biological age (regional curve, RC in red) shown together with the 95% bootstrap confidence range (grey).* ***e****, The number of MXD measurement series calculated for each year over the first 300 years of biological age.*

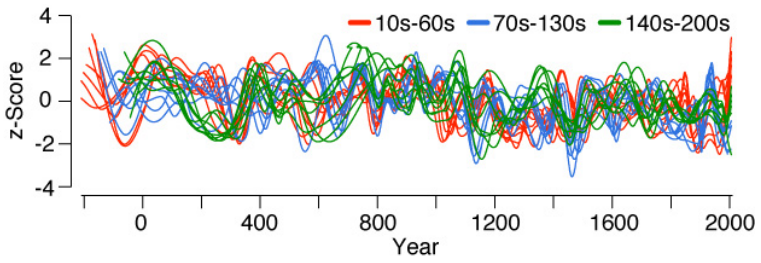

Figure S8. *Signal coherence among tree-ring age classes. Coloured curves are 100-year spline filters fit to 21 sub-samples of the long-term N-Scan MXD data. The sub-samples represent biological age classes 1-10 years, 11-20 years, ..., 61-70 years (in red), 71-80 years ..., 131-140 years (in blue), and 141-150 years, ..., 201-210 years (in green). The MXD data were RCS-detrended, and splines normalized over individual record lengths. See ref. 13 for details on age-class separation and spline fitting procedures.*

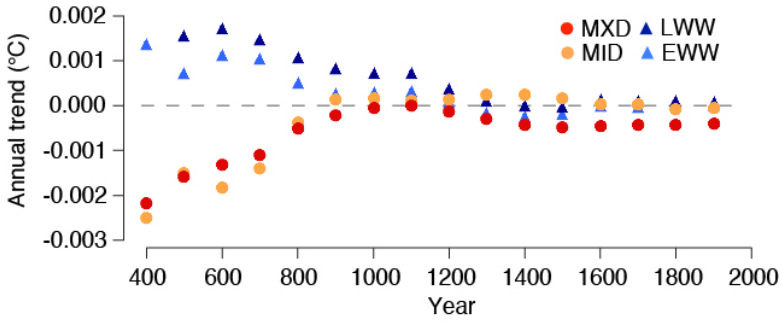

Figure S9. *Trends in tree-ring parameters. The figure shows the annual trends of linear regression slopes over the 138 BC to AD 1900 (symbols at 1900), 138 BC to AD 1800 (symbols at 1800), ..., 138 BC to AD 400 (symbols at 400) periods of maximum latewood density (MXD), minimum latewood density (MID), earlywood width (EWW), and latewood width (LWW) chronologies derived from the N-Scan data. All chronologies were detrended using the RCS method.*

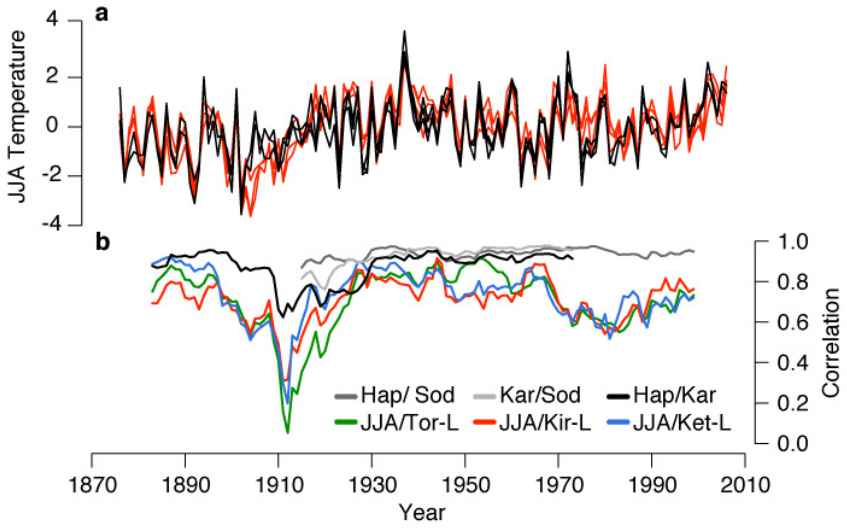

Figure S10. *Regional climate data and correlation with proxy records.* ***a****, JJA mean temperatures recorded in Haparanda, Karasjok, and Sodankyla (black curves) together with the Ket-L, Kir-L, and Tor-L MXD chronologies (red curves). The tree-ring data have been scaled to the mean of the three temperature timeseries over the 1876-2006 period. All records are shown as anomalies with respect to 1951-1980 mean temperatures.* ***b****, 15-year running correlations between the temperature station records (grey curves), and between the tree-ring and mean station data (coloured curves).*

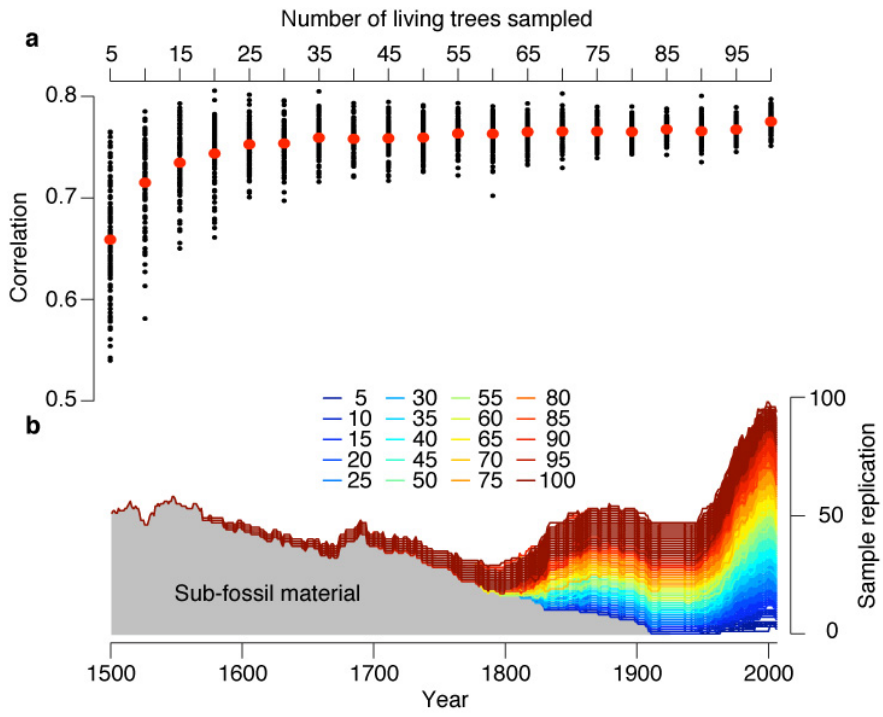

Figure S11. *Influence of sample replication on calibration against instrumental temperatures.* ***a****, Correlation coefficients of MXD chronologies developed using 5, 10, 15, ...100 series randomly drawn from the population of living trees (215 series) in conjunction with the full relict population (372 series) in RCS detrendings. For each replication level the procedure was repeated 100 times (black) together with the mean correlation (red). Correlations were computed over the 1876-2006 period with JJA mean temperatures averaged from the Haparanda, Karasjok, and Sodankyla stations.* ***b****, Changing sample replication of the 2000 MXD chronologies used in* ***a****, with colouring denoting the number of living series sampled. Red (e.g., 100 series) sample replication curves are overlaid upon the blue (e.g., 10 living series) curves.*

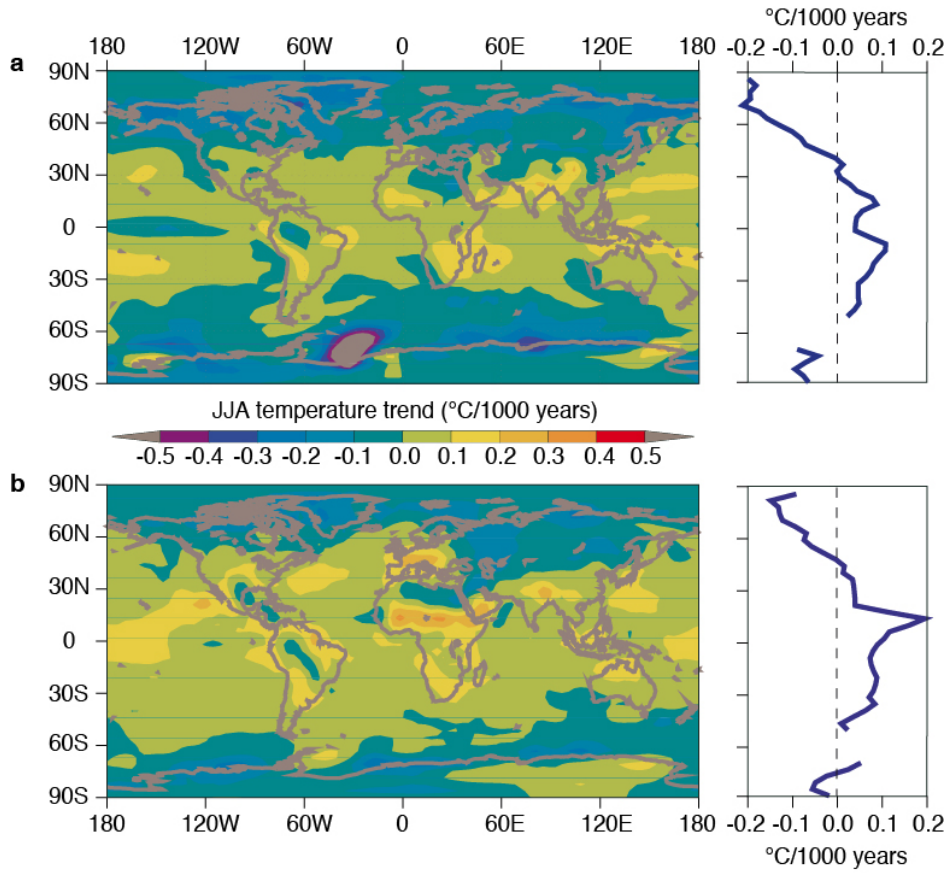

Figure S12. *Orbitally forced temperature trends in coupled global climate models (CGCMs). Maps show simulated JJA temperature trends over the AD 1-1900 period derived from multi-millennial* ***a****, ECHO-G Oetzi1 and* ***b****, ECHAM5/MPIOM runs with and without orbital forcing. Right panels show the zonal mean temperature trends per 1000 years averaged over continental land areas (no values at ~ 60°S).*

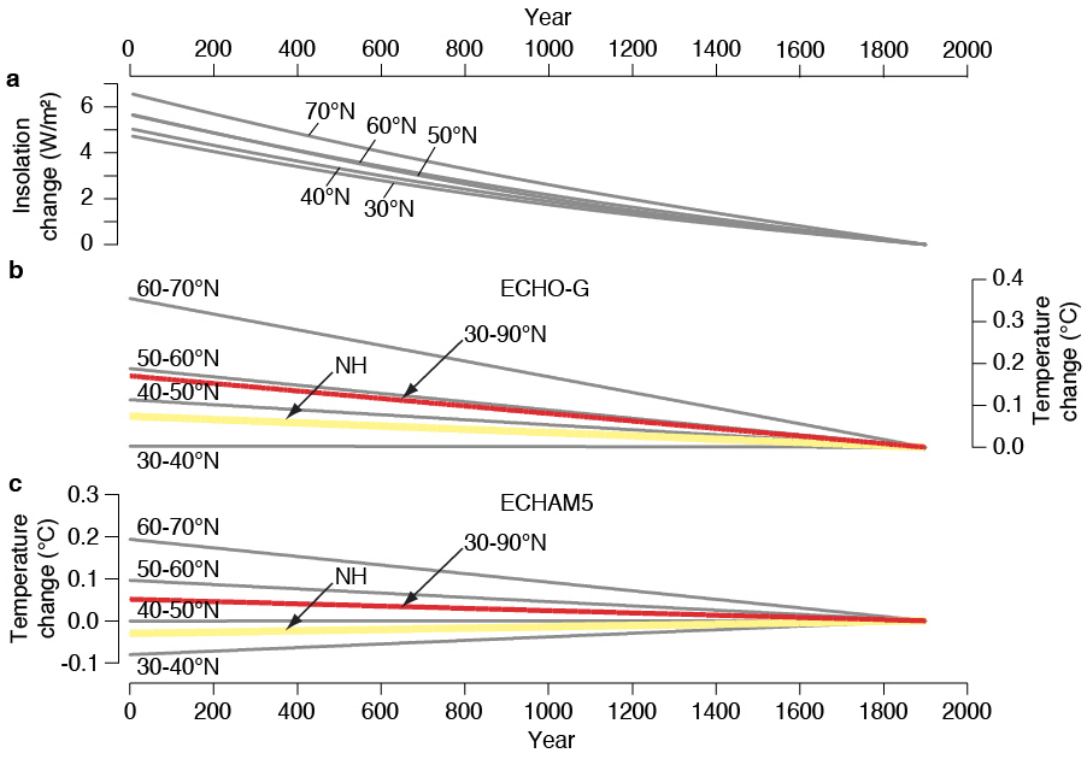

Figure S13. *Latitudinal insolation and simulated temperature trends over the Common Era.* ***a****, JJA insolation changes (in W/m²) in 30°, 40°, ..., 70°N relative to AD 1900.* ***b****, JJA temperature trends in latitudinal bands 30-40°N, 40-50°N, ..., 60-70°N, as well as 30-90°N and the full NH derived from the orbitally forced ECHO-G CGCM.* ***c****, Same as in* ***b****, but for the ECHAM5/MPIOM model.*

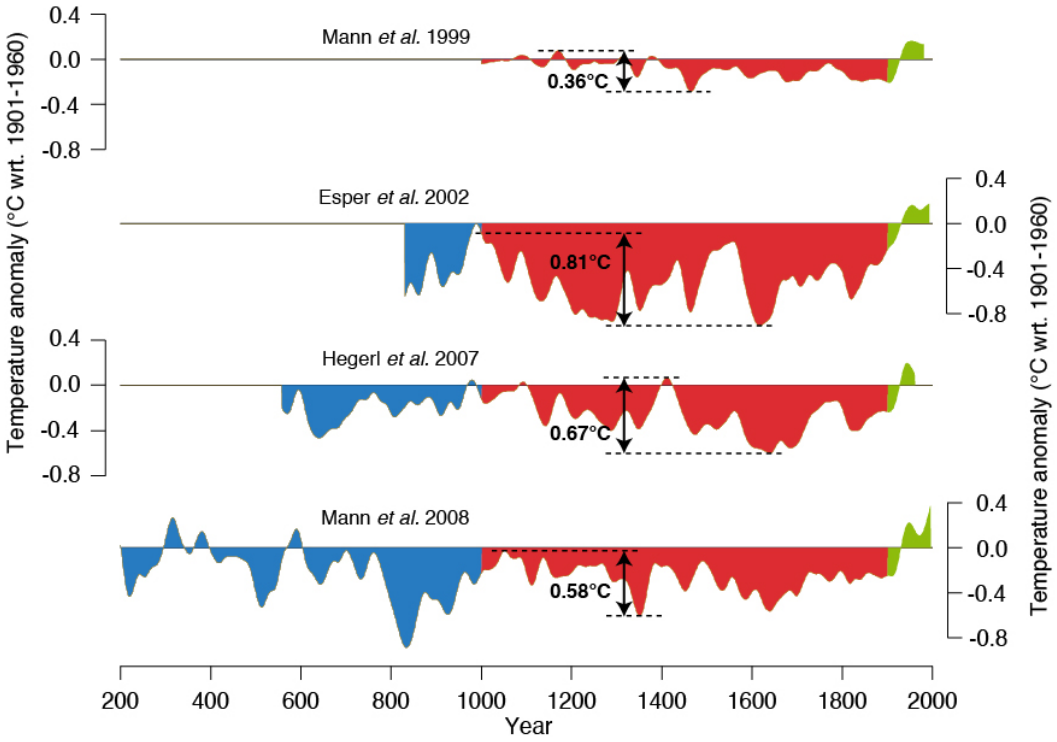

Figure S14. *Temperature variations over the past 1000 to 1800 years as revealed in large-scale temperature reconstructions that are dominated by NH extratropical tree-ring data*[14-17]*. All records were smoothed using a 50-year low pass filter. First millennium AD shown in blue, second millennium AD (until 1900) in red, 20th century data in green. Arrows indicate maximum temperature differences (of the smoothed curves) during the AD 1001-1900 period.*

Supplementary References

1. Grudd, H., Briffa, K. R., Karlén, W., Bartholin, T. S., Jones, P. D. & Kromer, B. A 7400-year tree-ring chronology in northern Swedish Lapland: Natural climate variability expressed on annual to millennial time scales. *Holocene* **12**, 657–665 (2002).
2. Helama S., Macias Fauria M., Mielikäinen K., Timonen M. & Eronen M. 2010: Sub-Milankovitch solar forcing of past climates: mid and late Holocene perspectives. *Geol. Soc. Am. Bull.* **122**, 1981–1988 (2010).
3. Hantemirov, R. M. & Shiyatov, S. G. A continuous multimillennial ring-width chronology in Yamal, northwestern Siberia. *Holocene* **12**, 717–726 (2002)
4. Bakke, J., Dahl, S. O., Paasche, Ø., Løvlie, R., & Nesje, A. Glacier fluctuations, equilibrium-line altitudes and palaeoclimate in Lyngen, northern Norway, during the Lateglacial and Holocene. *Holocene* **15**, 518–540 (2005).
5. Bakke, J., Lie, Ø., Nesje, A., Dahl, S. O. & Paasche, Ø. Utilizing physical sediment variability in glacier-fed lakes for continuous glacier reconstructions during the Holocene, northern Folgefonna, western Norway. *Holocene* **15**, 161–176 (2005).
6. MacDonald, G. M., Kremenetski, K. V. & Beilman, D. W. Climate change and the northern Russian treeline zone. *Phil. Trans. R. Soc. B* **363**, 2285–2299 (2008).
7. Zorita, E., Gonzlez-Rouco, F., von Storch, H., Montavez, J. P. & Valero, F. Natural and anthropogenic modes of surface temperature variations in the last thousand years. *Geophys. Res. Lett.* **32**, L08707, doi: 10.1029/2004GL021563 (2005).
8. Min, S.-K., Legutke, S., Hense, A. & Kwon, W. T. Internal variability in a 1000-yr control simulation with the coupled climate model ECHO-G. *Tellus* **57A**, 605–621 (2005).
9. Fischer, N. & Jungclaus, J. H. Evolution of the seasonal temperature cycle in a transient Holocene simulation: orbital forcing and sea-ice. *Clim. Past* **7**, 1139–1148 (2011).
10. Gleckler, P. J., Taylor, K. E. & Doutriaux, C. Performance metrics for climate models. *J. Geophys. Res.* **113**, D06104, doi: 10.1029/2007JD008972 (2008).
11. Cook, E. R. & Kairiukstis L. A. *Methods of dendrochronology – applications in the environmental science.* (Kluwer Academic Publishers, 1990).
12. Wigley, T. M. L., Briffa, K. R. & Jones, P. D. On the average of value of correlated time series, with applications in dendroclimatology and hydrometeorology. *J. Clim. Appl. Meteor.* **23**, 201–213 (1984).
13. Esper, J., Krusic, P. Peters, K. & Frank, D. Exploration of long-term growth changes using the tree-ring detrending program Spotty. *Dendrochronologia* **27**, 75–82 (2009).
14. Esper, J., Cook, E. & Schweingruber, F. Low-frequency signals in long tree-ring chronologies for reconstructing past temperature variability. *Science* **295**, 2250–2253 (2002).
15. Hegerl , G. C. *et al.* Detection of human influence on a new, validated 1500-year temperature reconstruction. *J. Clim.* **20**, 650–666 (2007).
16. Mann, M. E., Bradley, R. S. & Hughes, M. K. Northern hemisphere temperatures during the past millennium: inferences, uncertainties, and limitations. *Geophys. Res. Lett.* **26**, 759–762 (1999).
17. Mann, M. E. *et al.* Proxy-based reconstructions of hemispheric and global surface temperature variations over the past two millennia. *Proc. Natl. Acad. Sci. USA* **105**, 13252–13257 (2008).